

# Towards Ground Truth for Single Image Deraining

Yunhao Ba<sup>1\*</sup>, Howard Zhang<sup>1\*</sup>, Ethan Yang<sup>1</sup>, Akira Suzuki<sup>1</sup>, Arnold Pfahnl<sup>1</sup>,  
Chethan Chinder Chandrappa<sup>1</sup>, Celso de Melo<sup>2</sup>, Suya You<sup>2</sup>, Stefano Soatto<sup>1</sup>,  
Alex Wong<sup>1</sup>, and Achuta Kadambi<sup>1</sup>

<sup>1</sup> University of California, Los Angeles  
{yhba,hwd15508,eyang657,asuzuki100,ajpfahnl,chinderc}@ucla.edu  
{soatto,alexw}@cs.ucla.edu  
achuta@ee.ucla.edu

<sup>2</sup> DEVCOM Army Research Laboratory  
{celso.m.demelo.civ,suya.you.civ}@army.mil

**Abstract.** We propose a large-scale dataset of real-world rainy and clean image pairs and a method to remove degradations, induced by rain streaks and rain accumulation, from the image. As there exists no real-world dataset for deraining, current state-of-the-art methods rely on synthetic data and thus are limited by the sim2real domain gap; moreover, rigorous evaluation remains a challenge due to the absence of a real paired dataset. We fill this gap by collecting the first real paired deraining dataset through meticulous control of non-rain variations. Our dataset enables paired training and quantitative evaluation for diverse real-world rain phenomena (e.g. rain streaks and rain accumulation). To learn a representation invariant to rain phenomena, we propose a deep neural network that reconstructs the underlying scene by minimizing a rain-invariant loss between rainy and clean images. Extensive experiments demonstrate that the proposed dataset benefits existing derainers, and our model can outperform the state-of-the-art deraining methods on real rainy images under various conditions.

**Keywords:** Single-image rain removal, Real deraining dataset

## 1 Introduction

Single-image deraining aims to remove degradations induced by rain from images. Restoring rainy images can not only improve their aesthetic properties, but also supports reuse of abundant publicly available pretrained models across computer vision tasks. Top performing methods use deep networks, but suffer from a common issue: it is not possible to obtain ideal real ground-truth pairs of rain and clean images. The same scene, in the same space and time, cannot be observed both with and without rain. To overcome this, deep learning based rain removal relies on synthetic data.

---

\* Equal contribution.

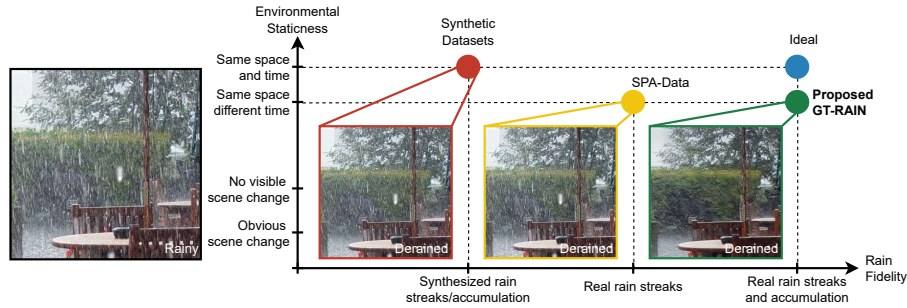


**Fig. 1. The points above depict datasets and their corresponding outputs from models trained on them.** These outputs come from a real rain image from the Internet. In contrast to folk wisdom, our opinion\* is that GT-RAIN is the right dataset for the deraining community because it has a smaller domain gap to the ideal ground truth. \* Why an asterisk? The asterisk emphasizes that this is an “opinion”. It is impossible to quantify the domain gap because collecting true real data is infeasible. To date, deraining is largely a viewer’s imagination of what the derained scene should look like. Therefore, we present the derained images above and leave it to the viewer to judge the gap. Additionally GT-RAIN, the first and only real approximation, can be used in complement with the litany of synthetic datasets [30,52,12,56,57,28,18].

The use of synthetic data for deraining is very prevalent [30,52,57,56,12,28,18]. However, current rain simulators cannot model all the complex effects of rain, which leads to unwanted artifacts when applying models trained on them to real-world rainy scenes. For instance, a number of synthetic methods add *rain streaks* to clean images to generate the pair [30,52,12,56,57], but rain does not only manifest as streaks: If raindrops are further away, the streaks meld together, creating *rain accumulation*, or *veiling* effects, which are exceedingly difficult to simulate. A further challenge with synthetic data is that results on real test data can only be evaluated qualitatively, for no real paired ground truth exists.

Realizing these limitations of synthetic data, we tackle the problem from another angle by relaxing the concept of ideal ground truth to a sufficiently short time window (see Fig. 1). We decide to conduct the experiment of obtaining short time interval paired data, particularly in light of the timely growth and diversity of landscape YouTube live streams. We strictly filter such videos with objective criteria on illumination shifts, camera motion, and motion artifacts. Further correction algorithms are applied for subtle variations, such as slight movements of foliage. We call this dataset GT-RAIN, as it is a first attempt to provide real paired ground truth for deraining. Although our dataset relies on streamers, YouTube’s fair use policy allows its release to the academic community. Please refer to Fig. 1 for an illustration of a comparison between GT-RAIN and other existing datasets.

**Defining “real, paired ground truth”:** Clearly, obtaining real, paired ground truth data by capturing a rain and rain-free image pair at the exact same space

and time is not feasible. However, the dehazing community has accepted several test sets [3,4,1,2] following these guidelines as a satisfactory replacement for evaluation purposes:

- A pair of degraded and clean images is captured as real photos at two different timestamps;
- Illumination shifts are limited by capturing data on cloudy days;
- The camera configuration remains identical while capturing the degraded and clean images.

We produce the static pairs in GT-RAIN by following the above criterion set forth by the dehazing community while enforcing a stricter set of rules on sky and local motion. More importantly, as a further step closer towards obtaining real ground truth pairs, we capture natural weather effects instead, which address problems of scale and variability that inherently come with simulating weather through man-made methods. We demonstrate that on average, methods trained on our proposed dataset improve in performance by 1dB. Additionally, in the results of the proposed method, we not only see quantitative and qualitative improvements, but also showcase a unique ability to handle diverse rain physics that could not previously be handled through synthetic methods.

### 1.1 Contributions

In summary, we make the following contributions:

- We propose a real-world paired dataset: GT-RAIN. The dataset captures *real* rain phenomena, from rain streaks to accumulation under various rain fall conditions, to bridge the domain gap that is too complex to be modeled by synthetic [30,52,57,56,12,28,18] and semi-real [46] datasets.
- We introduce an avenue for the deraining community to now have standardized quantitative and qualitative evaluations. Previous evaluations were quantifiable only wrt. simulations.
- We propose a framework to reconstruct the underlying scene by learning representations invariant to the rain phenomena via a rain-invariant loss function. Our approach outperforms the state of the art [55] by 12.3% PSNR on average for deraining real images.

## 2 Related Work

**Rain physics:** Raindrops exhibit diverse physical properties while falling, and many experimental studies have been conducted to investigate these, including the equilibrium shape [5], size [37], terminal velocity [14,10], spatial distribution [36], and temporal distribution [58]. A mixture of these distinct properties transforms the photometry of a raindrop into a complex mapping of the environmental radiance which considers refraction, specular reflection, and internal reflection [13]:

$$L(\hat{n}) = L_r(\hat{n}) + L_s(\hat{n}) + L_p(\hat{n}), \quad (1)$$

**Table 1. Our proposed large-scale dataset enables paired training and quantitative evaluation for real-world deraining.** We consider SPA-Data [46] as a semi-real dataset since it only contains real rainy images, where the pseudo ground-truth images are synthesized from a rain streak removal algorithm.

Dataset	Type	Rain Effects	Size
Rain12 [30]	Simulated	Synth. streaks only	12
Rain100L [52]	Simulated	Synth. streaks only	300
Rain800 [57]	Simulated	Synth. streaks only	800
Rain100H [52]	Simulated	Synth. streaks only	1.9K
Outdoor-Rain [28]	Simulated	Synth. streaks & Synth. accumulation	10.5K
RainCityscapes [18]	Simulated	Synth. streaks & Synth. accumulation	10.62K
Rain12000 [56]	Simulated	Synth. streaks only	13.2K
Rain14000 [12]	Simulated	Synth. streaks only	14K
NYU-Rain [28]	Simulated	Synth. streaks & Synth. accumulation	16.2K
SPA-Data [46]	Semi-real	Real streaks only	29.5K
<b>Proposed</b>	<b>Real</b>	<b>Real streaks &amp; Real accumulation</b>	<b>31.5K</b>

where  $L(\hat{n})$  is the radiance at a point on the raindrop surface with normal  $\hat{n}$ ,  $L_r(\cdot)$  is the radiance of the refracted ray,  $L_s(\cdot)$  is the radiance of the specularly reflected ray, and  $L_p(\cdot)$  is the radiance of the internally reflected ray. In real images, the appearance of rain streaks is also affected by motion blur and background intensities. Moreover, the dense rain accumulation results in sophisticated veiling effects. Interactions of these complicated phenomena make it challenging to simulate realistic rain effects on real images. Until GT-RAIN, previous works [46,22,45,55,15,28,19] have relied heavily on simulated rain and are limited by the sim2real gap.

**Deraining datasets:** Most data-driven deraining models require paired rainy and clean, rain-free ground-truth images for training. Due to the difficulty of collecting real paired samples, previous works focus on synthetic datasets, such as Rain12 [30], Rain100L [52], Rain100H [52], Rain800 [57], Rain12000 [56], Rain14000 [12], NYU-Rain [28], Outdoor-Rain [28], and RainCityscapes [18]. Even though synthetic images from these datasets incorporate some physical characteristics of real rain, significant gaps still exist between synthetic and real data [53]. More recently, a “paired” dataset with real rainy images (SPA-Data) was proposed in [46]. However, their “ground-truth” images are in fact a product of a video-based deraining method – synthesized based on the temporal motions of raindrops which may introduce artifacts and blurriness; moreover, the associated rain accumulation and veiling effects are not considered. In contrast, we collect pairs of real-world rainy and clean ground-truth images by enforcing rig-

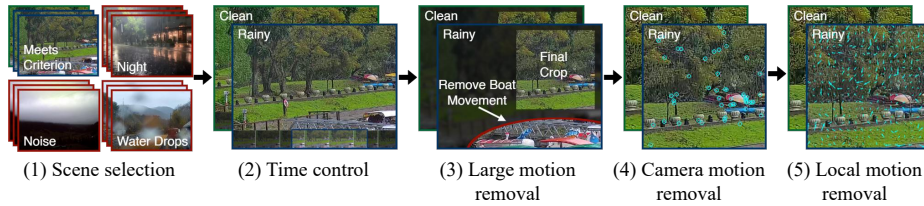


**Fig. 2. We collect the first real paired deraining dataset by rigorously controlling the environmental variations.** First, we remove heavily degraded videos such as scenes without proper exposure, noise, or water droplets on the lens. Next, we carefully choose the rainy and clean frames as close as possible in time to mitigate illumination shifts before cropping to remove large movement. Lastly, we correct for small camera motion (due to strong wind) using SIFT [32] and RANSAC [9] and perform elastic image registration [43,44] by estimating the displacement field when necessary.

orous selection criteria to minimize the environmental variations. To the best of our knowledge, our dataset is the first large-scale dataset with real paired data. Please refer to Table 1 for a detailed comparison of the deraining datasets.

**Single-image deraining:** Many previous methods used model-based solutions to derain [30,34,7,23]. More recently, deep-learning based methods [45,41,39,56,52,11,22,55,46,15,28,19] have seen increasing popularity and progress. The multi-scale progressive fusion network (MSPFN) [22] characterizes and reconstructs rain streaks at multiple scales. The rain convolutional dictionary network (RCDNet) [45] encodes the rain shape using the intrinsic convolutional dictionary learning mechanism. The multi-stage progressive image restoration network (MPRNet) [55] splits the image into different sections in various stages to learn contextualized features at different scales. The spatial attentive network (SPANet) [46] learns physical properties of rain streaks in a local neighborhood and reconstructs the clean background using non-local information. EfficientDeRain (EDR) [15] aims to derain efficiently in real time by using pixel-wise dilation filtering. Other than rain streak removal, the heavy rain restorer (HRR) [28] and the depth-guided non-local network (DGNet) [19] have also attempted to address rain accumulation effects. All of these prior methods use synthetic or semi-real datasets, and show limited generalizability to real images. In contrast, we propose a derainer that learns a rain-invariant representation via contrastive loss from real images.

### 3 Dataset

We now describe our method to control variations in a real dataset of paired images taken at two different timestamps, as illustrated in Fig. 2.

**Data collection:** We collect rain and clean ground-truth videos using a Python program based on FFmpeg to download videos from YouTube live streams across

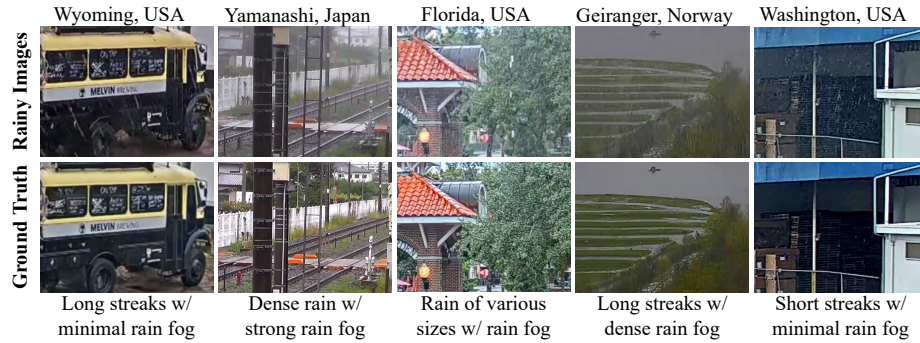


**Fig. 3.** Our proposed dataset contains diverse rainy images collected across the world. We illustrate several representative image pairs with various rain streak appearances and rain accumulation strengths at different geographic locations.

the world. For each live stream, we record the location in order to determine whether there is rain according to the OpenWeatherMap API [33]. In addition, we determine the time of day to filter out nighttime videos. After the rain stops, we continue downloading from the live stream in order to collect clean ground-truth frames. We note that while our dataset is formatted for single-image deraining tasks, it can be re-purposed for video deraining as well by considering the timestamps of the frames collected.

**Collection criteria:** To minimize variations between rainy and clean frames, videos are filtered based on a strict set of collection criteria. Note that we perform realignment for camera and local motion only when necessary – with manual oversight to filter out cases where motion still exists after realignment. Please see examples of motion correction and alignment in the supplement.

- **Heavily degraded scenes** that contain excessive noise, webcam artifacts, poor resolution, or poor camera exposure are filtered out as the underlying scene cannot be inferred from the images.
- **Water droplets** on the surface of the lens occlude large portions of the scene and also distort the image. Images containing this type of degradation are filtered out as it is out of the scope of this work – we focus on rain streak and rain accumulation phenomena.
- **Illumination shifts** are mitigated by minimizing the time difference between rainy and clean frames. Our dataset has an average time difference of 25 minutes, which drastically limits large changes in global illumination due to sun position, clouds, etc.
- **Background changes** containing large discrepancies (e.g cars, people, swaying foliage, water surfaces) are cropped from the frame to ensure that clean and rainy images are aligned. By limiting the average time difference between scenes, we also minimize these discrepancies before filtering. All sky regions are cropped out as well to ensure proper background texture.

- **Camera motion.** Adverse weather conditions, such as heavy wind, can cause camera movements between the rainy and clean frames. To address this, we use the Scale Invariant Feature Transform (SIFT) [32] and Random Sample Consensus (RANSAC) [9] to compute the homography matrix to realign the frames.
- **Local motion.** Despite controlling for motion whenever possible, certain scenes still contain small local movements that are unavoidable, especially in areas of foliage. To correct for this, we perform elastic image registration when necessary by estimating the displacement field [43,44].

**Dataset statistics:** Our large-scale dataset includes a total of 31,524 rainy and clean frame pairs, which is split into 26,124 training frames, 3,300 validation frames, and 2,100 testing frames. These frames are taken from a total of 101 videos covering a large variety of background scenes from urban locations (e.g. buildings, streets, cityscapes) to natural scenery (e.g. forests, plains, hills). We cover a wide range of geographic locations from around the world (e.g. North America, Europe, Oceania, Asia) to ensure that we capture diverse scenes and rain fall conditions. The scenes also include varying degrees of illumination from different times of day. The webcams cover a wide array of resolutions, noise levels, intrinsic parameters (focal length, optical center, distortion), etc. We include rain of varying densities, streak lengths, shapes, and sizes. As a result, our dataset incorporates diverse rain effects that cannot be accurately reproduced by SPA-Data [46] or synthetic datasets [30,52,57,56,12,28,18]. Please refer to Fig. 3 for an illustration of several image pairs in GT-RAIN.

## 4 Learning to Derain Real Images

To handle greater diversity of rain streak appearance, we propose a method to learn a representation that is invariant to rain for real image deraining. Our framework is illustrated in Fig. 4.

### 4.1 Problem Formulation

Most existing derainers emphasize on the rain streak removal and rely on the following equation to model the real-world rain phenomenon [30,61,12,27,56,8,54,46,45]:

$$\mathbf{I} = \mathbf{J} + \sum_i^n \mathbf{S}_i, \quad (2)$$

where  $\mathbf{I} \in \mathbb{R}^{3 \times H \times W}$  is the observed rainy image,  $\mathbf{J} \in \mathbb{R}^{3 \times H \times W}$  is the rain-free or “clean” image, and  $\mathbf{S}_i$  is the  $i$ -th rain layer. However, real-world rain can be more complicated due to the dense rain accumulation and the rain veiling effect [51,28,29]. These additional effects, which are visually similar to fog and mist, may cause severe image degradation, and thus removing them should

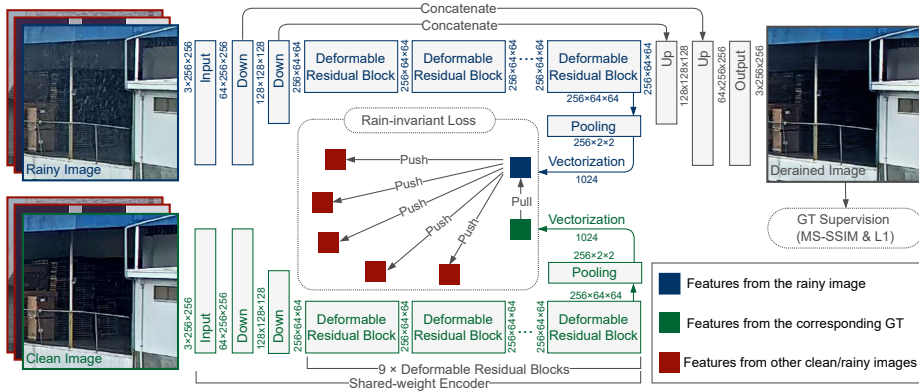


**Fig. 4. By minimizing a rain-invariant objective, our model learns robust features for reconstruction.** When training, a shared-weight encoder is used to extract features from rainy and ground-truth images. These features are then evaluated with the rain-invariant loss, where features from a rainy image and its ground-truth are encouraged to be similar. Learned features from the rainy images are also fed into a decoder to reconstruct the ground-truth images with MS-SSIM and  $\ell_1$  loss functions.

also be a primary goal for single-image deraining. With GT-RAIN, it now becomes possible to study and conduct optically challenging, real-world rainy image restoration.

Given an image  $\mathbf{I}$  of a scene captured during rain, we propose to learn a function  $\mathcal{F}(\cdot, \theta)$  parameterized by  $\theta$  to remove degradation induced by the rain phenomena. This function is realized as a neural network (see Fig. 4) that takes as input a rainy image  $\mathbf{I}$  and outputs a “clean” image  $\hat{\mathbf{J}} = \mathcal{F}(\mathbf{I}, \theta) \in \mathbb{R}^{3 \times H \times W}$ , where undesirable characteristics, i.e. rain streaks and rain accumulation, are removed from the image to reconstruct the underlying scene  $\mathbf{J}$ .

## 4.2 Rain-invariant Loss

To derain an image  $\mathbf{I}$ , one may directly learn a map from  $\mathbf{I}$  to  $\hat{\mathbf{J}}$  simply by minimizing the discrepancies between  $\hat{\mathbf{J}}$  and the ground truth  $\mathbf{J}$ , i.e. an image reconstruction loss – such is the case for existing methods. Under this formulation, the model must explore an infinitely large hypothesis space, e.g. any region obscured by rain streaks is inherently ambiguous, making learning difficult.

Unlike previous works, we constrain the learned representation such that it is invariant to rain phenomena. To “learn away” the rain, we propose to map both the rainy and clean images of the same scene to an embedding space where they are close to each other by optimizing a similarity metric. Additionally, we minimize a reconstruction objective to ensure that the learned representation is sufficient to recover the underlying scene. Our approach is inspired by the recent advances in contrastive learning [6], and to the best of our knowledge, it is the first attempt to distill rain-invariant representations of real-world scenes by

directly comparing the rainy and clean images in the feature space. But unlike [6], we do not define a positive pair as augmentation to the same image, but rather any rainy image and its corresponding clean image from the same scene.

When training, we first randomly sample a mini-batch of  $N$  rainy images with the associated clean images to form an augmented batch  $\{(\mathbf{I}_i, \mathbf{J}_i)\}_{i=1}^N$ , where  $\mathbf{I}_i$  is the  $i$ -th rainy image, and  $\mathbf{J}_i$  is its corresponding ground-truth image. This augmented batch is fed into a shared-weight feature extractor  $\mathcal{F}_E(\cdot, \theta_E)$  with weights  $\theta_E$  to obtain a feature set  $\{(\mathbf{z}_{\mathbf{I}_i}, \mathbf{z}_{\mathbf{J}_i})\}_{i=1}^N$ , where  $\mathbf{z}_{\mathbf{I}_i} = \mathcal{F}_E(\mathbf{I}_i, \theta_E)$  and  $\mathbf{z}_{\mathbf{J}_i} = \mathcal{F}_E(\mathbf{J}_i, \theta_E)$ . We consider every  $(\mathbf{z}_{\mathbf{I}_i}, \mathbf{z}_{\mathbf{J}_i})$  as the positive pairs. This is so that the learned features from the same scene should be close to each other regardless of the rainy conditions. We treat the other  $2(N-1)$  samples from the same batch as negative samples. Based on the noise-contrastive estimation (NCE) [16], we adopt the following InfoNCE [38] criterion to measure the rain-invariant loss for a positive pair  $(\mathbf{z}_{\mathbf{J}_i}, \mathbf{z}_{\mathbf{I}_i})$ :

$$\ell_{\mathbf{z}_{\mathbf{J}_i}, \mathbf{z}_{\mathbf{I}_i}} = -\log \frac{\exp(\text{sim}_{\cos}(\mathbf{z}_{\mathbf{I}_i}, \mathbf{z}_{\mathbf{J}_i})/\tau)}{\sum_{\mathbf{k} \in \mathcal{K}} \exp(\text{sim}_{\cos}(\mathbf{z}_{\mathbf{J}_i}, \mathbf{k})/\tau)}, \quad (3)$$

where  $\mathcal{K} = \{\mathbf{z}_{\mathbf{I}_j}, \mathbf{z}_{\mathbf{J}_j}\}_{j=1, j \neq i}^N$  is a set that contains the features extracted from other rainy and ground-truth images in the selected mini-batch,  $\text{sim}_{\cos}(\mathbf{u}, \mathbf{v}) = \mathbf{u}^T \mathbf{v} / \|\mathbf{u}\| \|\mathbf{v}\|$  is the cosine similarity between two feature vectors  $\mathbf{u}$  and  $\mathbf{v}$ , and  $\tau$  is the temperature parameter [50]. We set  $\tau$  as 0.25, and this loss is calculated across all positive pairs within the mini-batch for both  $(\mathbf{z}_{\mathbf{I}_i}, \mathbf{z}_{\mathbf{J}_i})$  and  $(\mathbf{z}_{\mathbf{J}_i}, \mathbf{z}_{\mathbf{I}_i})$ .

### 4.3 Full Objective

While minimizing Eq. (3) maps features of clean and rainy images to the same subspace, we also need to ensure that the representation is sufficient to reconstruct the scene. Hence, we additionally minimize a Multi-Scale Structural Similarity Index (MS-SSIM) [48] loss and a  $\ell_1$  image reconstruction loss to prevent the model from discarding useful information for the reconstruction task. Our full objective  $\mathcal{L}_{\text{full}}$  is as follows:

$$\mathcal{L}_{\text{full}}(\hat{\mathbf{J}}, \mathbf{J}) = \mathcal{L}_{\text{MS-SSIM}}(\hat{\mathbf{J}}, \mathbf{J}) + \lambda_{\ell_1} \mathcal{L}_{\ell_1}(\hat{\mathbf{J}}, \mathbf{J}) + \lambda_{\text{invariant}} \mathcal{L}_{\text{invariant}}(\mathbf{z}_{\mathbf{J}}, \mathbf{z}_{\mathbf{I}}), \quad (4)$$

where  $\mathcal{L}_{\text{MS-SSIM}}(\cdot)$  is the MS-SSIM loss that is commonly used for image restoration [59],  $\mathcal{L}_{\ell_1}(\cdot)$  is the  $\ell_1$  distance between the estimated clean images  $\hat{\mathbf{J}}$  and the ground-truth clean images  $\mathbf{J}$ ,  $\mathcal{L}_{\text{invariant}}(\cdot)$  is the rain-invariant loss described in Sec. 4.2, and  $\lambda_{\ell_1}$  and  $\lambda_{\text{invariant}}$  are two hyperparameters to control the relative importance of different loss functions. In our experiments, we set both  $\lambda_{\ell_1}$  and  $\lambda_{\text{invariant}}$  as 0.1.

### 4.4 Network Architecture

We design our model based on the architecture introduced in [24,60]. As illustrated in Fig. 4, our network includes an encoder of one input convolutional

block, two downsampling blocks, and nine residual blocks [17] to yield latent features  $\mathbf{z}$ . This is followed by a decoder of two upsampling blocks and one output layer to map the features to  $\mathbf{J}$ . The input convolutional block contains two convolutional layers with kernel sizes of  $7 \times 7$  and  $3 \times 3$  respectively. The downsampling blocks are instantiated by  $3 \times 3$  convolutional layers with a stride of 2, and each upsampling block consists of a bilinear interpolation layer and a  $3 \times 3$  convolutional layer. Similar to the U-Net [42], we fuse outputs from the downsampling blocks to their corresponding upsampling blocks via  $3 \times 3$  convolutional layers to retain information lost in the bottleneck. Moreover, normal convolution layers are replaced by deformable convolution layers [62] in our residual blocks— in doing so, we enable our model to propagate non-local spatial information to reconstruct local degradations caused by rain effects. We use batch normalization [21] and choose leaky ReLUs [35] with a negative slope of 0.1 as the activation function. Latent features  $\mathbf{z}$  are used for the rain-invariant loss described in Eq. (3). Since these features are high dimensional ( $256 \times 64 \times 64$ ), we use an average pooling layer to condense the feature map of each channel to  $2 \times 2$ . The condensed features are flattened into a vector of length 1024 for the rain-invariant loss (see Fig. 4). It is worth noting that our rain-invariant loss does not require additional modifications on the model architectures.

#### 4.5 Implementation Details

Our deraining model is trained on  $256 \times 256$  patches and a mini-batch size  $N = 8$  for 20 epochs. We use the Adam optimizer [26] with  $\beta_1 = 0.9$  and  $\beta_2 = 0.999$ . The initial learning rate is  $2 \times 10^{-4}$ , and it is steadily modified to  $1 \times 10^{-6}$  based on a cosine annealing schedule [31]. We also use a linear warm-up policy for the first 4 epochs. For data augmentation, we use random cropping, random rotation, random horizontal and vertical flips, and RainMix augmentation [15]. Our model is implemented in PyTorch [40]. The MS-SSIM loss is implemented based on the PyTorch Image Quality (PIQ) library [25]. Experiments are conducted on an NVIDIA Tesla P100 GPU.

## 5 Experiments

We compare our method to state-of-the-art methods on GT-RAIN, both quantitatively and qualitatively, and Internet rainy images released by [49]. To quantify the difference between the derained results and the ground-truth images, we adopt peak signal-to-noise ratio (PSNR) [20] and structure similarity (SSIM) [47] metrics. We first demonstrate the domain gap between synthetic and real data in Sec. 5.1 and Sec. 5.2 by testing various derainers trained on the synthetic/semi-real datasets [30,12,52,57,46,18,28] on the GT-RAIN test set and Internet images. In Sec. 5.3, we also show that existing methods can benefit from GT-RAIN when trained from scratch on it.

### 5.1 Quantitative Evaluation on GT-RAIN

To quantify the sim2real gap between existing synthetic datasets, we test 7 representative existing state-of-the-art methods [46,28,22,45,19,15,55] on our GT-RAIN test set.<sup>3</sup> Since there exist numerous synthetic datasets [30,52,12,56,57,28,18] proposed by previous works, we found it intractable to train our method on each one and test on GT-RAIN; whereas, we found it more feasible to take the best derainers for each respective synthetic dataset and test on our proposed dataset as a proxy. This follows the conventions of previous deraining dataset papers [11,19,30,46,53,56,57] to compare with top performing methods from each existing dataset.

SPANet [46] is trained on SPA-Data [46]. HRR [28] utilizes both NYU-Rain [28] and Outdoor-Rain [28]. MSPFN [22] and MPRNet [55] are trained on a combination of multiple synthetic datasets [30,12,52,57]. DGNet [19] is trained on RainCityscapes [18]. For RCDNet [45] and EDR [15], multiple weights from different training sets are provided. We choose RCDNet [45] trained on SPA-Data [46] and EDR V4 [15] trained on Rain14000 [12] in the comparison for better performance.

Compared to training on the proposed dataset (ours, last column), methods trained on synthetic/semi-real data perform worse (Table 2), with the largest domain gap being in NYU-Rain and Outdoor-Rain (HRR) and RainCityscapes (DGNet). Two trends do hold: training on (1) more synthetic data gives better results (MSPFN, MPRNet) and (2) semi-real data also helps (SPANet). However, we note that even when multiple synthetic datasets [30,12,52,57] or semi-real dataset [46] are used, their performance on real data is still 2dB lower than training on GT-RAIN(ours).

Fig. 5 illustrates several representative derained images across scenarios with various rain appearance and rain accumulation densities. Training on GT-RAIN enables the network to remove most rain streaks and rain accumulation; whereas, training on synthetic/semi-real data tends to leave visible rain streaks. We note that HRR [28] and DGNet [19] may seem like they remove haze, but they in fact introduce undesirable artifacts into the image e.g. dark spots on the back of the traffic sign, tree, and sky. The strength of having ground-truth paired data is demonstrated by our 2.48 dB gain compared to the state of the art [55]. On test images with dense rain accumulation, the boost improves to 3.43 dB.

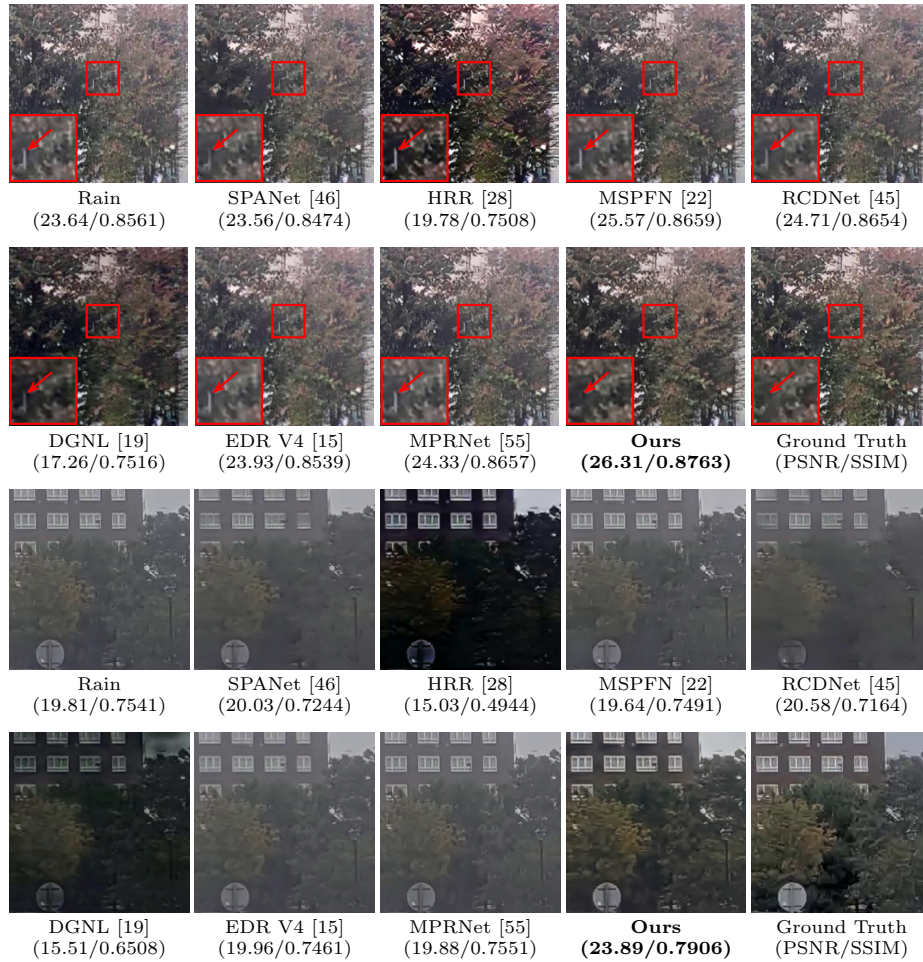
### 5.2 Qualitative Evaluation on Other Real Images

Other than the models described in Sec. 5.1, we also include EDR V4 [15] trained on SPA-Data [46] for the qualitative comparison, since it shows more robust rain streak removal results as compared the version trained on Rain14000 [12]. All the derained results on Internet rainy images are illustrated in Fig. 6. The model trained on the proposed GT-RAIN (i.e. ours) deals with large rain streaks of

<sup>3</sup> We use the original code and network weights from the authors for comparison. Code links for all comparison methods are provided in the supplementary material.

**Table 2. Quantitative comparison on GT-RAIN.** Our method outperforms the existing state-of-the-art derainers. The preferred results are marked in **bold**.

Data Split	Metrics	Rainy Images	SPANet [46] (CVPR'19)	HRR [28] (CVPR'19)	MSPFN [22] (CVPR'20)	RCDNet [45] (CVPR'20)	DGNL-Net [19] (IEEE TIP'21)	EDR [15] (AAAI'21)	MPRNet [55] (CVPR'21)	Ours
Dense Rain Streaks	PSNR $\uparrow$	18.66	18.87	17.86	19.58	19.50	17.33	18.86	19.12	<b>20.89</b>
	SSIM $\uparrow$	0.6445	0.6314	0.5872	0.6342	0.6218	0.5947	0.6296	0.6375	<b>0.6568</b>
Dense Rain Accumulation	PSNR $\uparrow$	21.24	21.42	14.82	21.13	21.27	20.75	21.07	21.38	<b>24.81</b>
	SSIM $\uparrow$	0.7768	0.7696	0.4675	0.7735	0.7765	0.7429	0.7766	0.7808	<b>0.8262</b>
Overall	PSNR $\uparrow$	19.76	19.96	16.55	20.24	20.26	18.80	19.81	20.09	<b>22.57</b>
	SSIM $\uparrow$	0.7012	0.6906	0.5359	0.6939	0.6881	0.6582	0.6926	0.6989	<b>0.7294</b>

**Fig. 5. Our model simultaneously removes rain streaks and rain accumulation, while the existing models fail to generalize to real-world data.** We select two representative scenes in the GT-RAIN test set (zoom to view details), and the associated PSNR and SSIM scores are listed at the bottom. The **red arrows** highlight the difference between the proposed method and others.

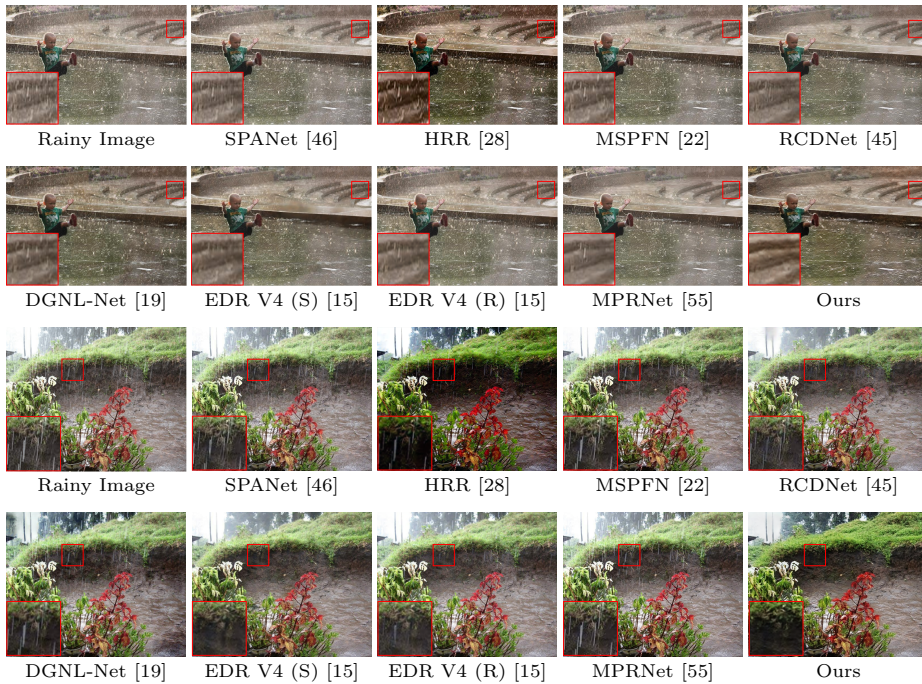


**Fig. 6. Our model is capable of generalizing to other real rainy images with robust performance.** We select representative real rainy images with various rain patterns and backgrounds for this qualitative (zoom to view details). EDR V4 (S) [15] denotes the EDR model trained on SPA-Data [46], and EDR V4 (R) [15] denotes the EDR model trained on Rain14000 [12].

various shapes and sizes as well as the associated rain accumulation effects, while preserving the features present in the scene. In contrast, we observe that models [28,19] trained on data with synthetic rain accumulation introduce unwanted color shifts and residual rain streaks in their results. Moreover, the state-of-the-art method [55] and top methods [22,45] are unable to remove the majority of rain streaks in general as highlighted in the red zoom boxes. This demonstrates the gap between top performers on synthetic versus one that can be applied to real data.

### 5.3 Training Methods on GT-RAIN

We additionally train several state-of-the-art derainers [45,15,55] on the GT-RAIN training set to demonstrate that our real dataset leads to more robust real-world deraining and benefits all models. We have selected the most recent derainers for this retraining study.<sup>4</sup> All the models are trained from scratch, and

<sup>4</sup> Both DGNL-Net [19] and HRR [28] cannot be retrained on our real dataset, as both require additional supervision, such as transmission maps and depth maps.

**Table 3. Training comparison methods on GT-RAIN.** The improvement of these derainers demonstrates the effectiveness of real paired data.

Data Split	Metrics	Rainy Images	RCDNet [45] (Original)	RCDNet [45] (GT-RAIN)	EDR [15] (Original)	EDR [15] (GT-RAIN)	MPRNet [55] (Original)	MPRNet [55] (GT-RAIN)	Ours
Dense Rain Streaks	PSNR $\uparrow$	18.66	19.50	19.60	18.86	19.95	19.12	20.19	<b>20.89</b>
	SSIM $\uparrow$	0.6445	0.6218	0.6492	0.6296	0.6436	0.6375	0.6542	<b>0.6568</b>
Dense Rain Accumulation	PSNR $\uparrow$	21.24	21.27	22.74	21.07	23.42	21.38	23.38	<b>24.81</b>
	SSIM $\uparrow$	0.7768	0.7765	0.7891	0.7766	0.7994	0.7808	0.8009	<b>0.8262</b>
Overall	PSNR $\uparrow$	19.76	20.26	20.94	19.81	21.44	20.09	21.56	<b>22.57</b>
	SSIM $\uparrow$	0.7012	0.6881	0.7091	0.6926	0.7104	0.6989	0.7171	<b>0.7294</b>

the corresponding PSNR and SSIM scores on the GT-RAIN test set are provided in Table 3. For all the retrained models, we can observe a PSNR and SSIM gain by using the proposed GT-RAIN dataset. In addition, with all models trained on the same dataset, our model comes out as the top performer in all categories.

**Table 4. Runtime comparison.** The average inference time is calculated on  $256 \times 256$  color images.

Model	SPANet [46] (CVPR'19)	HRR [28] (CVPR'19)	MSPFN [22] (CVPR'20)	RCDNet [45] (CVPR'20)	DGNL-Net [19] (IEEE TIP'21)	EDR [15] (AAAI'21)	MPRNet [55] (CVPR'21)	Ours
Number of Parameters	284k	40.6M	15.8M	3.16M	4.03M	27.3M	3.63M	12.9M
Inference Time (ms)	86.65	35.35	145.5	189.6	4.230	4.617	36.91	12.79

**Table 5. Ablation study.** Quantitative evaluation further validates the effectiveness of the rain-invariant loss.

Metrics	Rainy Images	Ours w/o $\mathcal{L}_{\text{invariant}}$	Ours w/ $\mathcal{L}_{\text{invariant}}$
PSNR $\uparrow$	19.76	21.69	<b>22.57</b>
SSIM $\uparrow$	0.7012	0.7193	<b>0.7294</b>

#### 5.4 Runtime Comparison

We list the total number of parameters with the associated runtime for other state-of-the-art methods and our proposed model in Table 4. The comparison is conducted on a single NVIDIA P100 GPU, and each derainer is asked to restore a colored rainy image of size  $256 \times 256$ . We note that the top three methods (DGNL-Net [19], EDR [15], and our proposed method) all operate at real-time deraining speeds. However, our method outperforms them by 3.77 dB and 2.76 dB PSNR respectively.

## 5.5 Ablation Study

We validate the effectiveness of the rain-invariant loss with two variants of the proposed method: (1) the proposed network with the full objective as describe in Sec. 4.3; and (2) the proposed network with just MS-SSIM loss and  $\ell_1$  loss. The rest of the training configurations and hyperparameters remain identical. The quantitative metrics for these two variants on the proposed GT-RAIN test set are listed in Table 5. Our model trained with the proposed rain-invariant loss consistently outperform the one without in both PSNR and SSIM.

## 6 Conclusions

Many of us in the deraining community probably wish for the existence of parallel universes, where we could capture the exact same scene with and without weather effects at the exact same time. Unfortunately, however, we are stuck with our singular universe, in which we are left with two choices: (1) synthetic data at the same timestamp with simulated weather effects or (2) real data at different timestamps with real weather effects. Though it is up to opinion, it is our belief that the results of our method in Fig. 6 reduce the visual domain gap more than those trained with synthetic datasets. Additionally, we hope the introduction of a real dataset opens up exciting new pathways for future work, such as the blending of synthetic and real data or setting goalposts to guide the continued development of improved simulators.

## References

1. Ancuti, C.O., Ancuti, C., Sbert, M., Timofte, R.: Dense-haze: A benchmark for image dehazing with dense-haze and haze-free images. In: 2019 IEEE international conference on image processing (ICIP). pp. 1014–1018. IEEE (2019)
2. Ancuti, C.O., Ancuti, C., Timofte, R.: Nh-haze: An image dehazing benchmark with non-homogeneous hazy and haze-free images. In: Proceedings of the IEEE/CVF Conference on Computer Vision and Pattern Recognition Workshops. pp. 444–445 (2020)
3. Ancuti, C.O., Ancuti, C., Timofte, R., De Vleeschouwer, C.: O-haze: a dehazing benchmark with real hazy and haze-free outdoor images. In: Proceedings of the IEEE conference on computer vision and pattern recognition workshops. pp. 754–762 (2018)
4. Ancuti, C., Ancuti, C.O., Timofte, R., Vleeschouwer, C.D.: I-haze: a dehazing benchmark with real hazy and haze-free indoor images. In: International Conference on Advanced Concepts for Intelligent Vision Systems. pp. 620–631. Springer (2018)
5. Beard, K.V., Chuang, C.: A new model for the equilibrium shape of raindrops. *Journal of Atmospheric Sciences* **44**(11), 1509–1524 (1987)
6. Chen, T., Kornblith, S., Norouzi, M., Hinton, G.: A simple framework for contrastive learning of visual representations. In: International conference on machine learning. pp. 1597–1607. PMLR (2020)

7. Chen, Y.L., Hsu, C.T.: A generalized low-rank appearance model for spatio-temporally correlated rain streaks. In: Proceedings of the IEEE International Conference on Computer Vision. pp. 1968–1975 (2013)
8. Deng, L.J., Huang, T.Z., Zhao, X.L., Jiang, T.X.: A directional global sparse model for single image rain removal. *Applied Mathematical Modelling* **59**, 662–679 (2018)
9. Fischler, M.A., Bolles, R.C.: Random sample consensus: a paradigm for model fitting with applications to image analysis and automated cartography. *Communications of the ACM* **24**(6), 381–395 (1981)
10. Foote, G.B., Du Toit, P.S.: Terminal velocity of raindrops aloft. *Journal of Applied Meteorology* **8**(2), 249–253 (1969)
11. Fu, X., Huang, J., Ding, X., Liao, Y., Paisley, J.: Clearing the skies: A deep network architecture for single-image rain removal. *IEEE Transactions on Image Processing* **26**(6), 2944–2956 (2017)
12. Fu, X., Huang, J., Zeng, D., Huang, Y., Ding, X., Paisley, J.: Removing rain from single images via a deep detail network. In: Proceedings of the IEEE/CVF Conference on Computer Vision and Pattern Recognition. pp. 3855–3863 (2017)
13. Garg, K., Nayar, S.K.: Vision and rain. *International Journal of Computer Vision* **75**(1), 3–27 (2007)
14. Gunn, R., Kinzer, G.D.: The terminal velocity of fall for water droplets in stagnant air. *Journal of Atmospheric Sciences* **6**(4), 243–248 (1949)
15. Guo, Q., Sun, J., Juefei-Xu, F., Ma, L., Xie, X., Feng, W., Liu, Y., Zhao, J.: Efficientderain: Learning pixel-wise dilation filtering for high-efficiency single-image deraining. In: Proceedings of the AAAI Conference on Artificial Intelligence. vol. 35, pp. 1487–1495 (2021)
16. Gutmann, M., Hyvärinen, A.: Noise-contrastive estimation: A new estimation principle for unnormalized statistical models. In: Proceedings of the thirteenth international conference on artificial intelligence and statistics. pp. 297–304. *JMLR Workshop and Conference Proceedings* (2010)
17. He, K., Zhang, X., Ren, S., Sun, J.: Deep residual learning for image recognition. In: Proceedings of the IEEE/CVF Conference on Computer Vision and Pattern Recognition. pp. 770–778 (2016)
18. Hu, X., Fu, C.W., Zhu, L., Heng, P.A.: Depth-attentional features for single-image rain removal. In: Proceedings of the IEEE/CVF Conference on Computer Vision and Pattern Recognition. pp. 8022–8031 (2019)
19. Hu, X., Zhu, L., Wang, T., Fu, C.W., Heng, P.A.: Single-image real-time rain removal based on depth-guided non-local features. *IEEE Transactions on Image Processing* **30**, 1759–1770 (2021)
20. Huynh-Thu, Q., Ghanbari, M.: Scope of validity of psnr in image/video quality assessment. *Electronics letters* **44**(13), 800–801 (2008)
21. Ioffe, S., Szegedy, C.: Batch normalization: Accelerating deep network training by reducing internal covariate shift. In: International conference on machine learning. pp. 448–456. *PMLR* (2015)
22. Jiang, K., Wang, Z., Yi, P., Chen, C., Huang, B., Luo, Y., Ma, J., Jiang, J.: Multi-scale progressive fusion network for single image deraining. In: Proceedings of the IEEE/CVF Conference on Computer Vision and Pattern Recognition. pp. 8346–8355 (2020)
23. Jiang, T.X., Huang, T.Z., Zhao, X.L., Deng, L.J., Wang, Y.: Fastderain: A novel video rain streak removal method using directional gradient priors. *IEEE Transactions on Image Processing* **28**(4), 2089–2102 (2018)

24. Johnson, J., Alahi, A., Fei-Fei, L.: Perceptual losses for real-time style transfer and super-resolution. In: Proceedings of the European Conference on Computer Vision. pp. 694–711. Springer (2016)
25. Kastruyulin, S., Zakirov, D., Prokopenko, D.: PyTorch Image Quality: Metrics and measure for image quality assessment (2019), <https://github.com/photosynthesis-team/piq>, open-source software available at <https://github.com/photosynthesis-team/piq>
26. Kingma, D.P., Ba, J.: Adam: A method for stochastic optimization. arXiv preprint arXiv:1412.6980 (2014)
27. Li, G., He, X., Zhang, W., Chang, H., Dong, L., Lin, L.: Non-locally enhanced encoder-decoder network for single image de-raining. In: Proceedings of the 26th ACM international conference on Multimedia. pp. 1056–1064 (2018)
28. Li, R., Cheong, L.F., Tan, R.T.: Heavy rain image restoration: Integrating physics model and conditional adversarial learning. In: Proceedings of the IEEE/CVF Conference on Computer Vision and Pattern Recognition. pp. 1633–1642 (2019)
29. Li, R., Tan, R.T., Cheong, L.F.: All in one bad weather removal using architectural search. In: Proceedings of the IEEE/CVF Conference on Computer Vision and Pattern Recognition. pp. 3175–3185 (2020)
30. Li, Y., Tan, R.T., Guo, X., Lu, J., Brown, M.S.: Rain streak removal using layer priors. In: Proceedings of the IEEE/CVF Conference on Computer Vision and Pattern Recognition. pp. 2736–2744 (2016)
31. Loshchilov, I., Hutter, F.: SGDR: stochastic gradient descent with warm restarts. In: 5th International Conference on Learning Representations, ICLR 2017, Toulon, France, April 24–26, 2017, Conference Track Proceedings. OpenReview.net (2017), <https://openreview.net/forum?id=Skq89Scxx>
32. Lowe, D.: Sift-the scale invariant feature transform. *Int. J* **2**(91-110), 2 (2004)
33. Ltd., O.: OpenWeatherMap API. <https://openweathermap.org/>, accessed: 2021-11-05
34. Luo, Y., Xu, Y., Ji, H.: Removing rain from a single image via discriminative sparse coding. In: Proceedings of the IEEE International Conference on Computer Vision. pp. 3397–3405 (2015)
35. Maas, A.L., Hannun, A.Y., Ng, A.Y.: Rectifier nonlinearities improve neural network acoustic models. In: in ICML Workshop on Deep Learning for Audio, Speech and Language Processing (2013)
36. Manning, R.M.: Stochastic Electromagnetic Image Propagation. McGraw-Hill Companies (1993)
37. Marshall, J., Palmer, W.M.: The distribution of raindrops with size. *Journal of Meteorology* **5**(4), 165–166 (1948)
38. Oord, A.v.d., Li, Y., Vinyals, O.: Representation learning with contrastive predictive coding. arXiv preprint arXiv:1807.03748 (2018)
39. Pan, J., Liu, S., Sun, D., Zhang, J., Liu, Y., Ren, J., Li, Z., Tang, J., Lu, H., Tai, Y.W., et al.: Learning dual convolutional neural networks for low-level vision. In: Proceedings of the IEEE/CVF Conference on Computer Vision and Pattern Recognition. pp. 3070–3079 (2018)
40. Paszke, A., Gross, S., Massa, F., Lerer, A., Bradbury, J., Chanan, G., Killeen, T., Lin, Z., Gimelshein, N., Antiga, L., Desmaison, A., Kopf, A., Yang, E., DeVito, Z., Raison, M., Tejani, A., Chilamkurthy, S., Steiner, B., Fang, L., Bai, J., Chintala, S.: Pytorch: An imperative style, high-performance deep learning library. In: Wallach, H., Larochelle, H., Beygelzimer, A., d'Alché-Buc, F., Fox, E., Garnett, R. (eds.) *Advances in Neural Information Processing Systems* 32, pp.

- 8024–8035. Curran Associates, Inc. (2019), <http://papers.neurips.cc/paper/9015-pytorch-an-imperative-style-high-performance-deep-learning-library.pdf>
41. Ren, D., Shang, W., Zhu, P., Hu, Q., Meng, D., Zuo, W.: Single image deraining using bilateral recurrent network. *IEEE Transactions on Image Processing* **29**, 6852–6863 (2020)
  42. Ronneberger, O., Fischer, P., Brox, T.: U-net: Convolutional networks for biomedical image segmentation. In: *International Conference on Medical image computing and computer-assisted intervention*. pp. 234–241. Springer (2015)
  43. Thirion, J.P.: Image matching as a diffusion process: an analogy with maxwell’s demons. *Medical image analysis* **2**(3), 243–260 (1998)
  44. Vercauteren, T., Pennec, X., Perchant, A., Ayache, N.: Diffeomorphic demons: Efficient non-parametric image registration. *NeuroImage* **45**(1), S61–S72 (2009)
  45. Wang, H., Xie, Q., Zhao, Q., Meng, D.: A model-driven deep neural network for single image rain removal. In: *Proceedings of the IEEE/CVF Conference on Computer Vision and Pattern Recognition* (June 2020)
  46. Wang, T., Yang, X., Xu, K., Chen, S., Zhang, Q., Lau, R.W.: Spatial attentive single-image deraining with a high quality real rain dataset. In: *Proceedings of the IEEE/CVF Conference on Computer Vision and Pattern Recognition*. pp. 12270–12279 (2019)
  47. Wang, Z., Bovik, A.C., Sheikh, H.R., Simoncelli, E.P.: Image quality assessment: from error visibility to structural similarity. *IEEE transactions on image processing* **13**(4), 600–612 (2004)
  48. Wang, Z., Simoncelli, E.P., Bovik, A.C.: Multiscale structural similarity for image quality assessment. In: *The Thirty-Seventh Asilomar Conference on Signals, Systems & Computers, 2003*. vol. 2, pp. 1398–1402. Ieee (2003)
  49. Wei, W., Meng, D., Zhao, Q., Xu, Z., Wu, Y.: Semi-supervised transfer learning for image rain removal. In: *Proceedings of the IEEE/CVF Conference on Computer Vision and Pattern Recognition*. pp. 3877–3886 (2019)
  50. Wu, Z., Xiong, Y., Yu, S.X., Lin, D.: Unsupervised feature learning via non-parametric instance discrimination. In: *Proceedings of the IEEE/CVF Conference on Computer Vision and Pattern Recognition*. pp. 3733–3742 (2018)
  51. Yang, W., Tan, R.T., Feng, J., Guo, Z., Yan, S., Liu, J.: Joint rain detection and removal from a single image with contextualized deep networks. *IEEE transactions on pattern analysis and machine intelligence* **42**(6), 1377–1393 (2019)
  52. Yang, W., Tan, R.T., Feng, J., Liu, J., Guo, Z., Yan, S.: Deep joint rain detection and removal from a single image. In: *Proceedings of the IEEE/CVF Conference on Computer Vision and Pattern Recognition*. pp. 1357–1366 (2017)
  53. Yang, W., Tan, R.T., Wang, S., Fang, Y., Liu, J.: Single image deraining: From model-based to data-driven and beyond. *IEEE Transactions on pattern analysis and machine intelligence* (2020)
  54. Yasarla, R., Patel, V.M.: Uncertainty guided multi-scale residual learning-using a cycle spinning cnn for single image de-raining. In: *Proceedings of the IEEE/CVF Conference on Computer Vision and Pattern Recognition*. pp. 8405–8414 (2019)
  55. Zamir, S.W., Arora, A., Khan, S., Hayat, M., Khan, F.S., Yang, M.H., Shao, L.: Multi-stage progressive image restoration. In: *Proceedings of the IEEE/CVF Conference on Computer Vision and Pattern Recognition*. pp. 14821–14831 (2021)
  56. Zhang, H., Patel, V.M.: Density-aware single image de-raining using a multi-stream dense network. In: *Proceedings of the IEEE/CVF Conference on Computer Vision and Pattern Recognition*. pp. 695–704 (2018)

57. Zhang, H., Sindagi, V., Patel, V.M.: Image de-raining using a conditional generative adversarial network. *IEEE transactions on circuits and systems for video technology* **30**(11), 3943–3956 (2019)
58. Zhang, X., Li, H., Qi, Y., Leow, W.K., Ng, T.K.: Rain removal in video by combining temporal and chromatic properties. In: 2006 IEEE international conference on multimedia and expo. pp. 461–464. IEEE (2006)
59. Zhao, H., Gallo, O., Frosio, I., Kautz, J.: Loss functions for image restoration with neural networks. *IEEE Transactions on computational imaging* **3**(1), 47–57 (2016)
60. Zhu, J.Y., Park, T., Isola, P., Efros, A.A.: Unpaired image-to-image translation using cycle-consistent adversarial networks. In: Proceedings of the IEEE International Conference on Computer Vision. pp. 2223–2232 (2017)
61. Zhu, L., Fu, C.W., Lischinski, D., Heng, P.A.: Joint bi-layer optimization for single-image rain streak removal. In: Proceedings of the IEEE International Conference on Computer Vision. pp. 2526–2534 (2017)
62. Zhu, X., Hu, H., Lin, S., Dai, J.: Deformable convnets v2: More deformable, better results. In: Proceedings of the IEEE/CVF Conference on Computer Vision and Pattern Recognition. pp. 9308–9316 (2019)

## Supplementary Material

### A Visualization of Previous Deraining Datasets

We illustrate some typical image pairs from various deraining datasets in Fig. 2. Synthetic datasets in the community are usually generated by adding synthetic rain effects on real images taken under sunny illumination conditions, and the semi-real SPA-Data [46] only considers rain streaks. As a result, the domain gap between these existing datasets and real rainy scenarios are relatively larger as compared with the proposed GT-RAIN dataset.

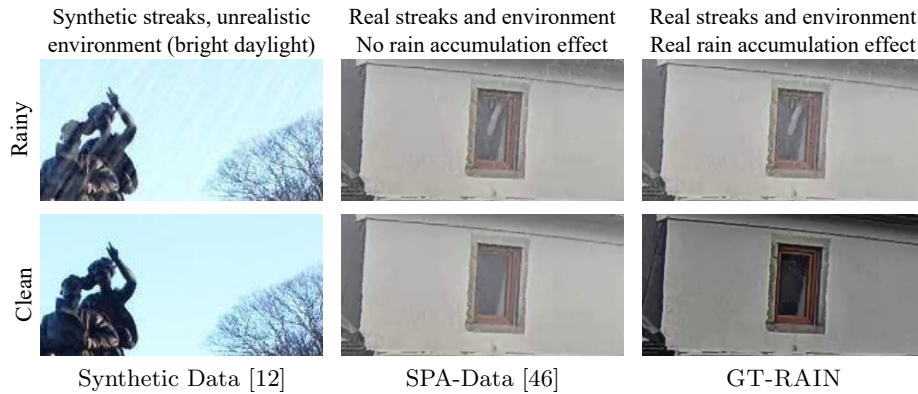


**Fig. A.** GT-RAIN contains realistic rain effects (both rain streaks and rain accumulation), while the existing synthetic and semi-real datasets fail to cover the physical complexity and diversity of real-world rain. The synthetic image pair is from the commonly used Rain14000 dataset [12], and the pseudo ground-truth image of SPA-Data [46] in the figure is generated by running the official code from the authors on our collected rainy video.

### B More Results from GT-RAIN

As an additional supplement to Fig. 5 in the main paper, we provide some more quantitative and qualitative results from our test set in Fig. B. Note that these comparison models are using the weights provided by the authors which are trained on synthetic or semi-real datasets. We see that our proposed model trained on GT-RAIN continues to outperform other competing models.

### C More Results on Internet Images

As a supplement to Fig. 6 in the main paper, we provide more qualitative results on real Internet images in Fig. C. Note that all comparison models are using the

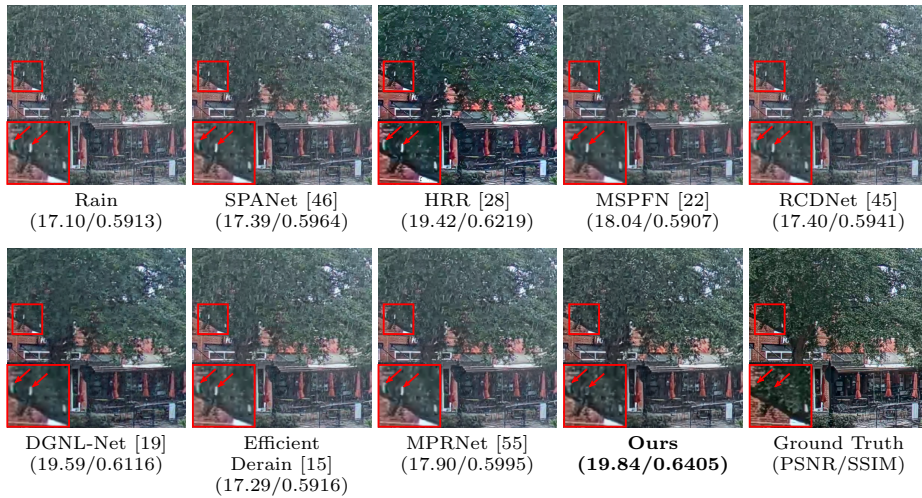


**Fig. B. More results on GT-RAIN test set.** Similarly, the proposed method is capable of removing various rain streaks and rain accumulation effects.

weights provided by the author, which are trained on synthetic or semi-real datasets. All images are taken from the dataset of common real rainy images provided by [49]. Our proposed model trained on GT-RAIN continues to remove rain streaks of varying shapes and sizes as well as rain accumulation without introducing the unwanted color shifts seen in HRR [28] and DGNL-Net [19].

## D Alignment of Small Motions

As a complement to Sec. 3 of the main paper, we first show, in Fig. D-(a), a ground-truth image overlaid on top of a rainy image to demonstrate representative samples that passed our data collection appearance criteria and also motion criterion, where we do not need to perform motion correction. We note that this is the case for the majority of our dataset. Additionally, we show an overlaid image pair that passed our appearance criteria, but failed the motion criterion. Fig. D-(b) shows the image pair before and after the motion correction. It should be noted that only a small portion of the data requires such correction, and our correction pipeline is designed to be robust to rain artifacts. It is because even though rain can influence local descriptors, the combinatorial matching stage is designed to be robust to a preponderance of outliers. For most cases, the percentage of outliers affects the time it takes to converge, but not the quality. All samples that require our correction procedure were manually inspected after the alignment – any failure cases of the procedure, typically due to extreme weather conditions, were manually removed.



**Fig. C. More qualitative results on Internet images.** Our model continues to exhibit robust generalization to real rainy images, whereas existing derainers usually fail on removing rain streaks of diverse shapes and sizes. EDR V4 (S) [15] denotes the EDR model trained on SPA-Data [46], and EDR V4 (R) [15] denotes the EDR model trained on Rain14000 [12].

## E Limitations

Although we achieve the state of the art for deraining real images, our method is not perfect. Our PSNR and SSIM scores on GT-RAIN are 22.57 dB and 0.7294. This suggests that indeed, we still have ample room for improvement. For example, we leave a slight rain accumulation in the tree in Fig. B. While the recovered image is sharper and contains less rain artifacts than competing

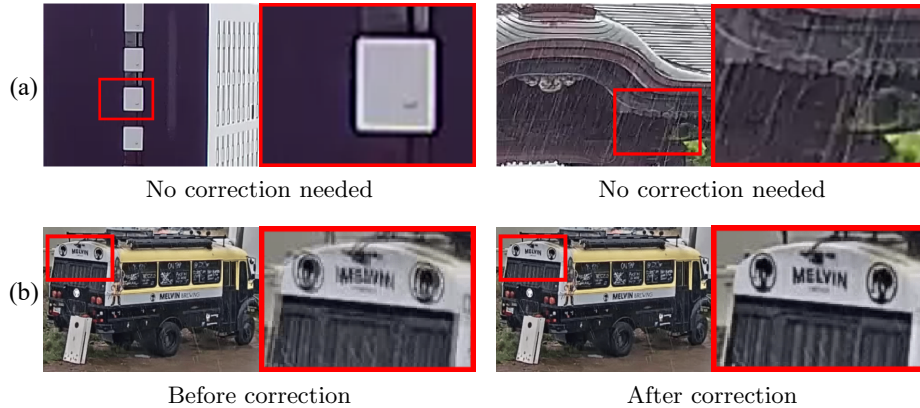


**Fig. D. The proposed method can correct for small motions under rain.** We illustrate two types of scenes by overlaying the rainy images on top of their clean ground truths: (a) two scenes that do not need additional image processing for motion alignment; and (b) a scene with motion before and after running the correction algorithms. It should be noted that both types of scenes are aligned properly in GT-RAIN.

methods, boundaries in highly textured areas (e.g. leaves, bricks, and foliage) are blurred. In Fig. C, we observe a similar trend. However, this is a challenge that plagues all methods. We hope that further extensions of our approach and GT-RAIN will help mitigate these artifacts. We also do not consider occlusions from raindrops on the camera lens because the raindrops will likewise be present on the lens after the rain stops. Moreover, we do not consider specular reflections from water surfaces. This is because these reflections are nearly impossible to reconstruct as the water ripples in the puddles will destroy the visual patterns during raining. We hope that future works can address these limitations.

## F Comparison Code Links

The code links for all the comparison methods are listed in Table A.

**Table A. Code links for the comparison methods.**

Methods	Links
SPANet [46] (CVPR'19)	<a href="https://github.com/stevewongv/SPANet">https://github.com/stevewongv/SPANet</a>
HRR [28] (CVPR'19)	<a href="https://github.com/liruoteng/HeavyRainRemoval">https://github.com/liruoteng/HeavyRainRemoval</a>
MSPFN [22] (CVPR'20)	<a href="https://github.com/kuijiang0802/MSPFN">https://github.com/kuijiang0802/MSPFN</a>
RCDNet [45] (CVPR'20)	<a href="https://github.com/hongwang01/RCDNet">https://github.com/hongwang01/RCDNet</a>
DGNL-Net [19] (IEEE TIP'21)	<a href="https://github.com/xw-hu/DGNL-Net">https://github.com/xw-hu/DGNL-Net</a>
Efficient Derain [15] (AAAI'21)	<a href="https://github.com/tsingqguo/efficientderain">https://github.com/tsingqguo/efficientderain</a>
MPRNet [55] (CVPR'21)	<a href="https://github.com/swz30/MPRNet">https://github.com/swz30/MPRNet</a>

## G Network Architecture

As an additional supplement of Sec. 4.4 in the main paper, we provide a detailed illustration of the network architecture in Table B.

**Table B. Illustration of our network architecture.**

Network	Kernel		Channels		Resolution		Parameters	Input
	Size	Stride	In	Out	In	Out		
<b>Encoder</b>								
InputConv1	7	1	3	64	1	1	$\approx 9.5\text{k}$	Rainy Image
InputConv2	3	1	64	64	1	1	$\approx 37.0\text{k}$	InputConv1
DownConv1	3	2	64	128	1	1/2	$\approx 74.0\text{k}$	InputConv2
DownConv2	3	2	128	256	1/2	1/4	$\approx 295.4\text{k}$	DownConv1
<b>DeformResBlock1</b>								
DeformConv11	3	1	256	256	1/4	1/4	$\approx 652.6\text{k}$	DownConv2
DeformConv12	3	1	256	256	1/4	1/4	$\approx 652.6\text{k}$	DeformConv11
Sum1	-	-	256	256	1/4	1/4	DownConv2 + DeformConv12	
<b>DeformResBlock2</b>								
DeformConv21	3	1	256	256	1/4	1/4	$\approx 652.6\text{k}$	Sum1
DeformConv22	3	1	256	256	1/4	1/4	$\approx 652.6\text{k}$	DeformConv21
Sum2	-	-	256	256	1/4	1/4	Sum1 + DeformConv21	
⋮								
<b>DeformResBlock9</b>								
DeformConv91	3	1	256	256	1/4	1/4	$\approx 652.6\text{k}$	Sum8
DeformConv92	3	1	256	256	1/4	1/4	$\approx 652.6\text{k}$	DeformConv91
Sum9	-	-	256	256	1/4	1/4	Sum8 + DeformConv92	
<b>Decoder</b>								
<b>UpConvBlock1</b>								
Bilinear1	-	-	256	256	1/4	1/2	-	Sum9
Conv11	3	1	256	128	1/2	1/2	$\approx 295.2\text{k}$	Bilinear2
Concat1	-	-	128 + 128	256	1/2	1/2	DownConv1, Conv11	
Conv12	3	1	256	128	1/2	1/2	$\approx 295.2\text{k}$	Concat1
<b>UpConvBlock2</b>								
Bilinear2	-	-	128	128	1/2	1	-	Conv12
Conv21	3	1	128	64	1	1	$\approx 73.9\text{k}$	Bilinear2
Concat2	-	-	64 + 64	128	1	1	InputConv2, Conv21	
Conv22	3	1	128	64	1	1	$\approx 73.9\text{k}$	Concat2
OutputConv	3	1	64	3	1	1	$\approx 1.7\text{k}$	Conv22
Total Parameters $\approx 12.9\text{M}$								